5

Effects of Bandwidth on Estimation of UWB Channel Parameters

Duje Čoko, Zoran Blažević and Ivan Marinović
University of Split
Faculty of Electrical Engineering, Mechanical Engineering and Naval Architecture
Croatia

1. Introduction

The subject of this chapter is to investigate the effect of bandwidth on a short range indoor UWB channel performance. This research is based on a measurement campaign performed on a wooden desk surface placed in an office room at our faculty building. A vector network analyzer (VNA) is used to sweep the 1 GHz, 2 GHz, 5 GHz and 7.5 GHz bandwidths centered at 6.85 GHz, obtaining the frequency response of the channel. Using the VNA time domain capability the channel impulse response is obtained. This is equivalent to sounding the channel with frequency chirp pulses equal in duration to the inverse of the frequency bandwidth. In other words, a narrower bandwidth results in a wider pulse in time domain.

Although the measurements are performed in same environment for all bandwidths, it is expected that an UWB channel itself would not be equally perceived by different pulse widths. A wider system bandwidth results in shorter pulses, which in turn account for finer temporal and spatial resolution. In this way more multipath components can be resolved as the pulses overlap in a lesser extent.

The fundamental differences between an UWB channel and a narrowband channel arise from the frequency selectivity of the propagation process (Molisch, 2005). As the UWB signal has a wide frequency spectrum which may extend to several gigahertz, the frequency dependence of diffraction/reflection coefficients and dielectric constants can be significant (Di Benedetto et al., 2006). A number of papers report on the effect of carrier frequency on channel parameters. One such investigation (Cassioli et al., 2004) finds a strong dependence between the path loss model exponent and the carrier frequency, yet states that there is no correlation with the bandwidth. (Ghassemzadeh et al., 2005) presented an extensive measurement campaign at two different bandwidths (1.25 GHz and 6 GHz) centered at 5 GHz, reporting mostly minor differences in parameter values between the two bandwidths. Another paper (Choi et al., 2009) models the path loss exponent variation as a function of frequency. A research project (Chang & Tarng, 2007) investigates the effects of bandwidth on observable multipath clustering and Δ-K model parameters for an indoor UWB wireless channel with signal bandwidths of 0.5, 1 and 2 GHz. However, to authors' knowledge, so far there have been no attempts to investigate the effects of bandwidth on estimating the path loss, shadowing, mean excess delay and RMS delay spread in short range UWB scenarios,

which are the key parameters for assessing the link budget, signal-to-noise ratio and intersymbol interference of the system.
The next section of the chapter explains the measurement procedure and equipment and describes the measurement environment. The subsequent sections present the path loss, shadowing, mean excess delay and RMS delay spread parameter values estimated from the measured power delay profiles, respectively. The obtained results are discussed in the seventh section. The chapter is concluded in the eighth section, briefly summarizing all the key findings of this research.

2. Experimental setup

The measurement campaign took place on an empty desk in one of the offices at our faculty building. The surface of the desk is cleared to ensure the line of sight (LOS) between the transmitter and the receiver. The desk used in measurements is made of wood, chipboard and MDF. Inner walls that separate offices and laboratories are mainly made of plasterboard constructed with a thin wire grid composition, while the external wall and floors are made of reinforced concrete. The floor is entirely covered with wooden parquetry. The doors are made of plywood, while the office furniture is made of various wooden materials and glass. In the vicinity of the desk on which the measurements are conducted is another desk with the measurement equipment and two cabinets in the bottom left corner of the office, as shown on the office plan on Fig. 1. This additional furniture in the office is introduced as an intentional scattering system to approximate a real-life scenario.

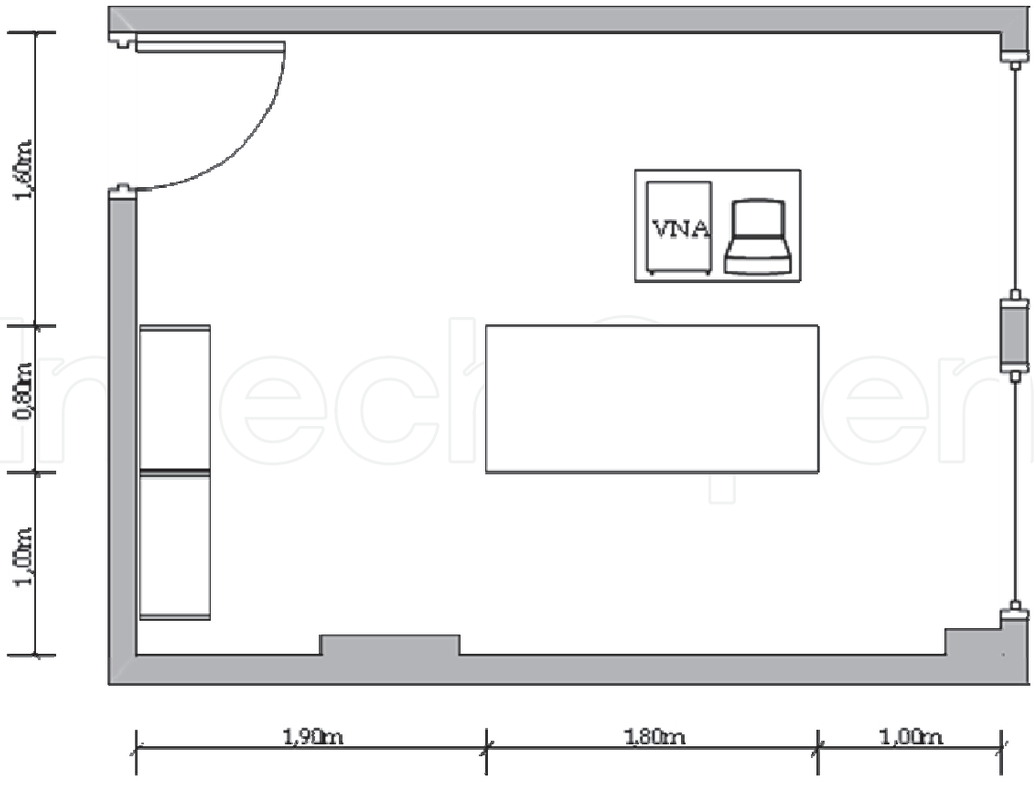

Fig. 1. Office plan

A 1.6 m x 0.7 m grid with 0.1 m spacing is drawn on a sheet of paper (Fig. 2) which is fixed on a surface of a plain office desk. This forms a matrix of 17 x 8 measurement points across the desktop. The transmitting antenna (presented by a red disk in Fig. 2) is placed on the top of the 9th column in a fixed position. The receiving antenna (presented by a blue disk in Fig. 2) is moved along the remaining 135 points for each measurement. Both antennas are erected on styrofoam blocks at the same height of 4.5 cm with their azimuth planes being parallel to the desk surface ($\Theta = 0°$).

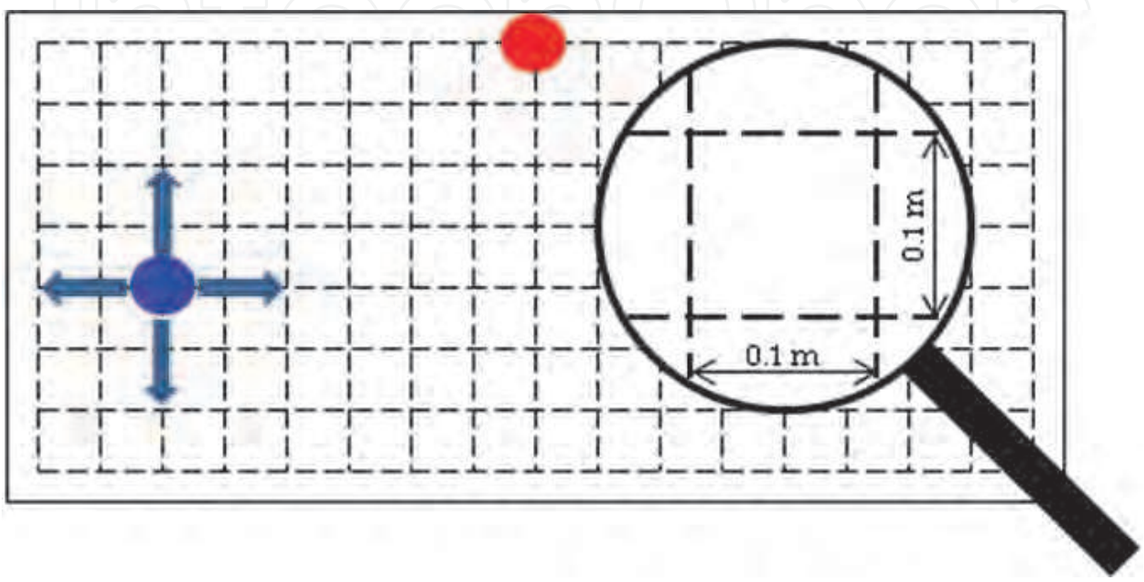

Fig. 2. Measurement grid and antenna positioning method. The red and blue disks present the transmitting antenna and the receiving antenna, respectively.

2.1 Measurement setup

The measurement setup is presented on Fig. 3. The transmitting antenna (Tx) is connected to the port 1 of the HP 8720A vector network analyzer (VNA) by a semi-rigid coaxial cable. The receiving antenna (Rx) is connected to the port 2 of the VNA by a flexible coaxial cable. The attenuation of the cables is compensated by the calibration procedure. The measured data from the VNA is transferred by the HP interface bus (HP-IB) to the data acquisition PC (PC-DAQ), where the data is stored for further processing.

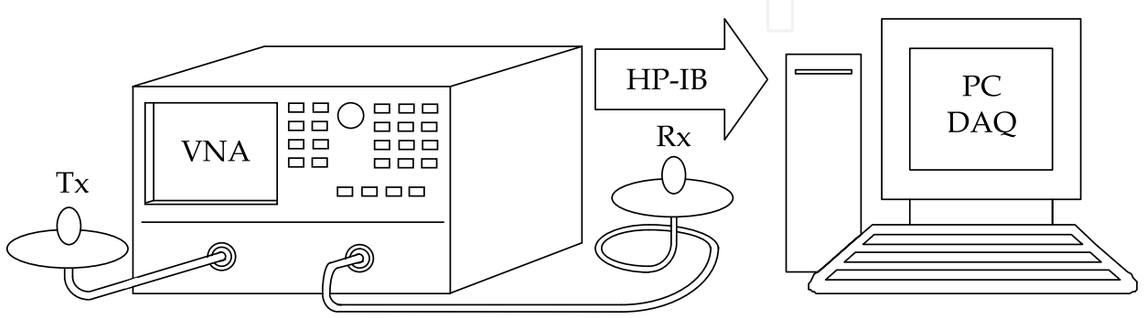

Fig. 3. Measurement setup

2.1.1 Vector network analyzer

A vector network analyzer (VNA) is used to measure the system's forward complex transmission coefficients $S_{21}(f_i)$ at 801 discrete evenly spaced frequencies within a given frequency span. In this way the band-limited transfer function of the system H is obtained:

$$H_{meas}(f) = W(f)H(f), \tag{1}$$

where H_{meas} is the measured transfer function and W is the selected transformation window of the VNA.

Using an inverse Fourier transform $\Im^{-1}$, the measurement results can be observed in the time delay domain, presenting the power delay profile (PDP) which gives the time distribution of the received signal power from a transmitted pulse:

$$\Im^{-1}\{H_{meas}(f)\} = h(\tau). \tag{2}$$

The measured data acquired from the VNA thus presents the frequency averaged power delay profiles.

The excess delay t is obtained by subtracting the time of arrival τ_0 of the first multipath component of the power delay profile from the time delay τ relative to the time instant of transmitting the pulse:

$$t = \tau - \tau_0. \tag{3}$$

By activating the VNA's averaging function, the last 16 measurements are averaged to reduce the temporal variations in the system. This results in a time averaged power delay profile:

$$P_h(t) = \frac{1}{N}\sum_{i=1}^{N}|h_i(t)|^2, \tag{4}$$

where N =16.

Prior to each measurement the VNA is calibrated using a specific calibration standard. The measured data is acquired via HP-IB interface to a PC for further analysis and correction. Before the parameter extraction procedure each measured PDP is corrected with respect to the predefined threshold, which was set to 5 dB above the noise level for all measured points. This correction sets all the delay bins with energies below this threshold to zero-energy bins.

2.1.2 Antennas

A pair of omnidirectional UWB antennas used in this measurement campaign was built according to the design proposed in (Taniguchi et al., 2006). To verify the omnidirectionality of the built antennas, their radiation patterns were measured in a TESEQ 750 GTEM cell at different frequencies generated by a HP 8340A synthesized sweeper. This method is based on measuring the power received by antenna under test (AUT) which is placed inside the cell. The received power was measured using a Rohde&Schwarz NRP-Z21 universal power sensor. Electric field in the vicinity of the AUT is measured by an isotropic electric field probe HI-4455 positioned next to the AUT. The antenna gain G in dBi is calculated using the following expression (Živković & Šarolić, 2010):

$$G = -162.8 + 20\log(f) + P_{rec} - E_i, \tag{5}$$

where f is the signal frequency in Hz, P_{rec} is the power received by AUT expressed in dBm, and E_i is the incident electric field in dBV/m. The radiation patterns measured at 4 GHz, 7 GHz and 10 GHz are presented on Fig. 4.

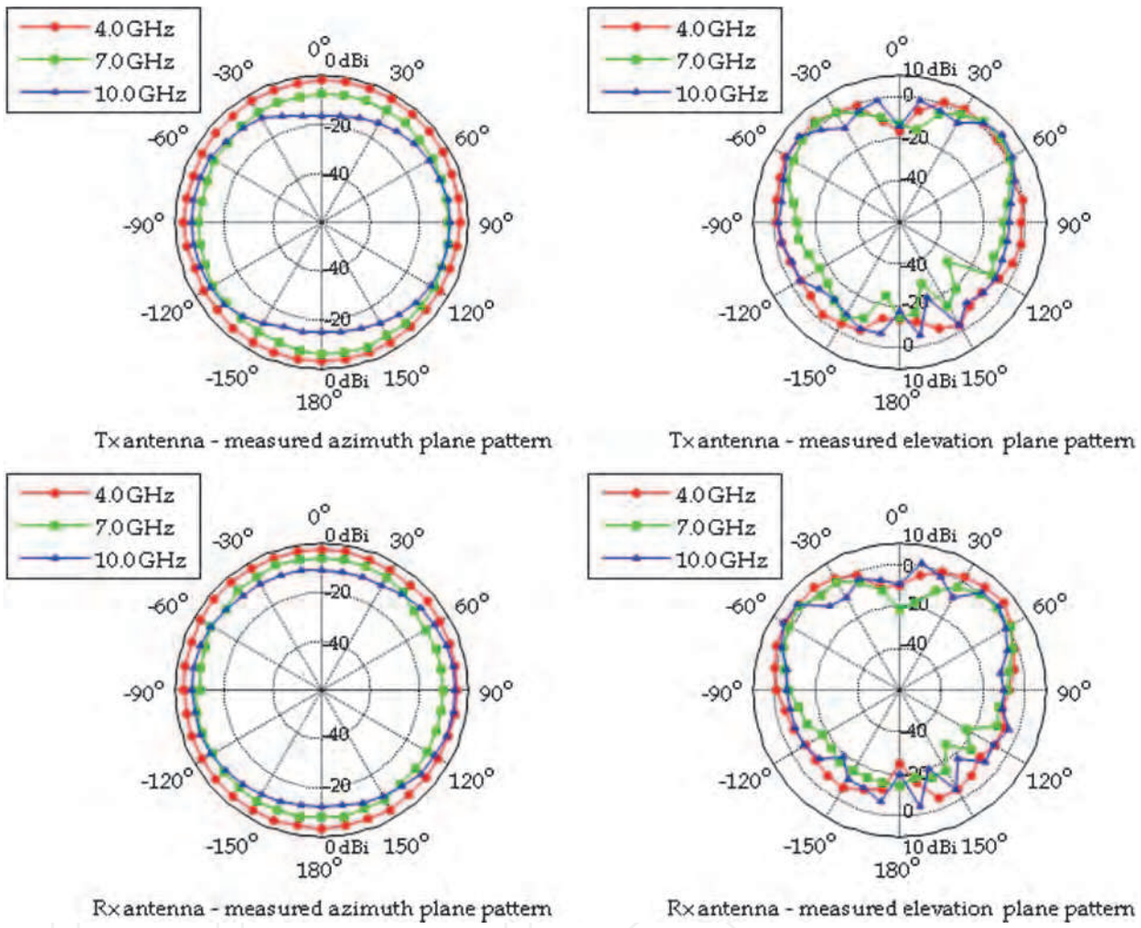

Fig. 4. Measured radiation patterns for both antennas at 4 GHz, 7 GHz and 10 GHz.

In addition, the VNA was used to measure the VSWR throughout the widest frequency bandwidth of 7.5 GHz, centered at 6.85 GHz. A full port calibration was performed before each measurement. The results, presented on Fig. 5, show that the VSWR is less than 2.5 throughout the entire frequency span.

Finally, the power delay profiles for different bandwidths were measured at a reference distance d_0 (= 0.1 m) at 0°, 45°, 90°, 135° and 180° in azimuth plane, while keeping both antennas at same height h (= 4.5 cm). Averaging the measured results and calculating the path loss from the power delay profile (Section 3) the total path loss at 0.1 m was estimated:

$$PL(d_0) = PL_{FS}(d_0) - G_r - G_t, \tag{6}$$

where PL_{FS} is the free space path loss, G_r and G_t are receiving and transmitting antenna gains, respectively, all expressed in dB.

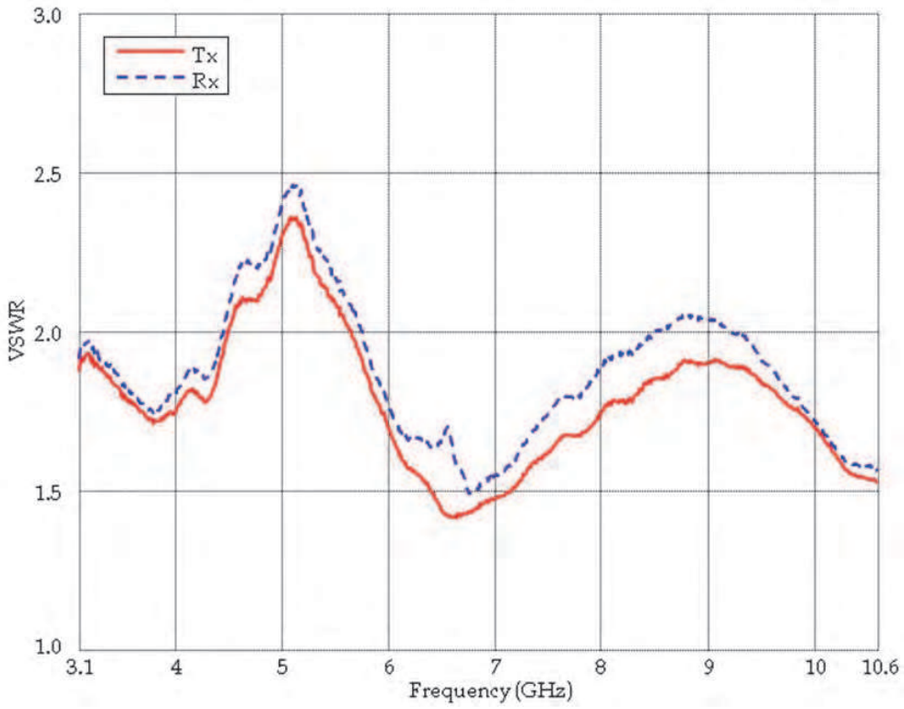

Fig. 5. Measured VSWR for both antennas vs. frequency.

Applying the Friis equation with f_c (= 6.85 GHz) as the center frequency, c (= 3*10^8 m/s) as the velocity of light and d_0 (= 0.1 m) as a referent antenna separation, the free space path loss is obtained:

$$PL_{FS}(d_0)[\text{dB}] = 20\log\left(\frac{4\pi f_c d_0}{c}\right) = 29.16 \text{ dB}. \tag{7}$$

Under the assumption that antenna gains are equal (G_r = G_t = G_a) we estimate the antenna gain within a given bandwidth:

$$G_a[\text{dB}] = \frac{PL_{FS}(d_0)[\text{dB}] - PL(d_0)[\text{dB}]}{2}. \tag{8}$$

The results are shown in Table 1.

Bandwidth	1 GHz	2 GHz	5 GHz	7.5 GHz
Antenna gain	-0.475 dB	-0.54 dB	-0.035dB	0.26 dB

Table 1. Estimated antenna gains at 0.1 m separation for different bandwidths.

The measurement results show that the antenna gain may be approximated to 0 dBi, implying a ±1 dB tolerance.

2.1.3 System resolution and dynamic range

After a preliminary observation of the power delay profiles on various measurement points at different bandwidths, it is noticed that the noise threshold is constant (slightly below -90

dB). Besides that, as the power in the profile decays with delay, there are no observable multipath components above the noise threshold approximately 60 ns after the time instant of transmitting the pulse for each bandwidth. According to this fact the display window from 0 ns to 80 ns is chosen for all considered bandwidths and measurement points. Since this window is sampled at 801 points, the display resolution for all measurements is 0.1 ns.

The temporal resolution of the measurement system is equal to the inverse of the bandwidth and has a value greater than the display resolution. Otherwise, the display window would exceed the maximum observable delay (Hovinen et al., 2002).

Once the VNA was calibrated, the pulse shape was observed it the time delay domain for each different bandwidth (Fig. 6). All pulses have a different peak value at $\tau = 0$, which is caused by normalizing the measurement results to the total energy of the pulse.

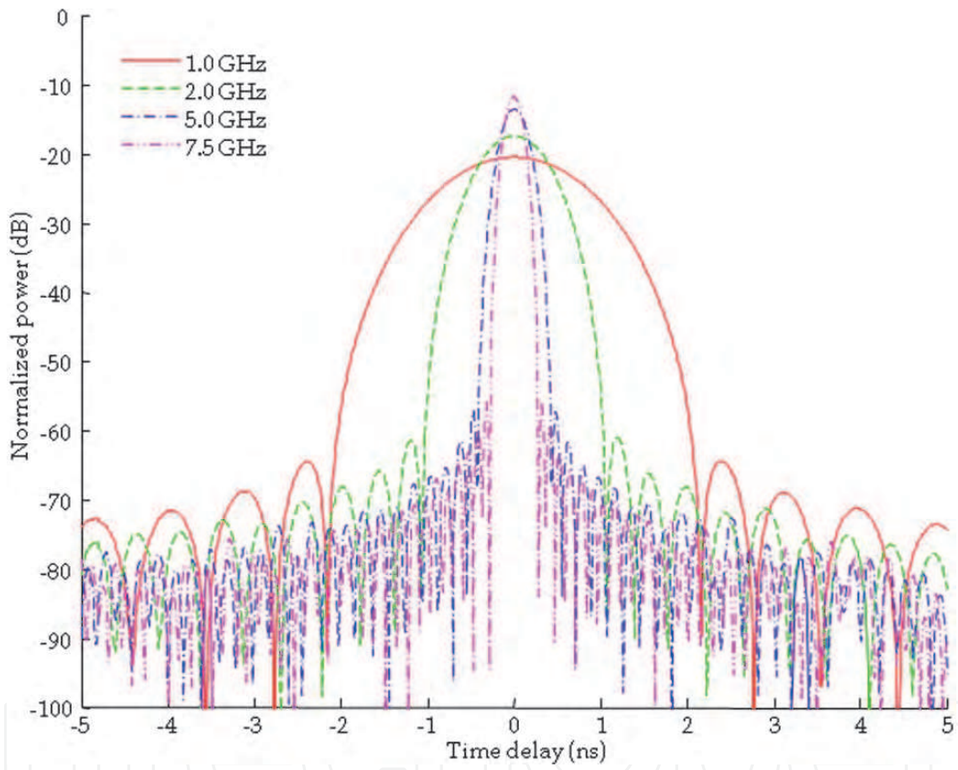

Fig. 6. The shape of the calibrated pulse for different bandwidths.

The VNA provides a windowing feature which is needed because of the abrupt transitions at the start and stop frequencies of the measured frequency span. The band limiting of a frequency domain response causes overshoot and ringing in a time domain response. This limits the usefulness of the time domain measurement in terms of the sidelobes and a pulse wider than the system resolution. The window used in the presented measurements is the normal window, which has a sidelobe level 44 dB below the pulse peak value and extends the pulse width to value of 3.84 times the system resolution for a bandpass mode (Hewlett-Packard Company, 1989). This has a direct consequence in spreading the pulse spatially, so that the spatial resolution of the system is degraded and the system can no longer resolve the multipath components with the precision expected from the system resolution. Another

consequence is that when observing the delays in relation to the time instant of the peak of the transmitted pulse, one can observe a certain amount of energy received in negative delay times. To eliminate this, several power delay profiles where the total energy was not captured are removed from the final set of measured data. Hence, the minimum measurement distance is half of the spatial width of the pulse at a given bandwidth.
Furthermore, the RMS delay spread is estimated for each pulse, as this value is to be subtracted from the measured RMS delay spread of each power delay profile (Section 6). The results are presented in Table 2.

Bandwidth	1 GHz	2 GHz	5 GHz	7.5 GHz
System resolution	1 ns	0.5 ns	0.2 ns	0.133 ns
Display resolution	0.1 ns	0.1 ns	0.1 ns	0.1 ns
Pulse width	3.84 ns	1.92 ns	0.768 ns	0.512 ns
Spatial width	1.152 m	0.576 m	0.23 m	0.154 m
Estimated pulse power	1.66 dB	1.66 dB	1.66 dB	1.66 dB
Pulse RMS delay spread	567 ps	283.4 ps	113.4 ps	75.6 ps

Table 2. System and pulse parameters for different bandwidths.

Fig. 7 shows a detail of normalized power profiles for different bandwidths. All the profiles are measured at 0.78 m antenna separation. It is evident that the measurement system with a narrow bandwidth cannot resolve as much multipath components as the same measurement system with wider bandwidth.

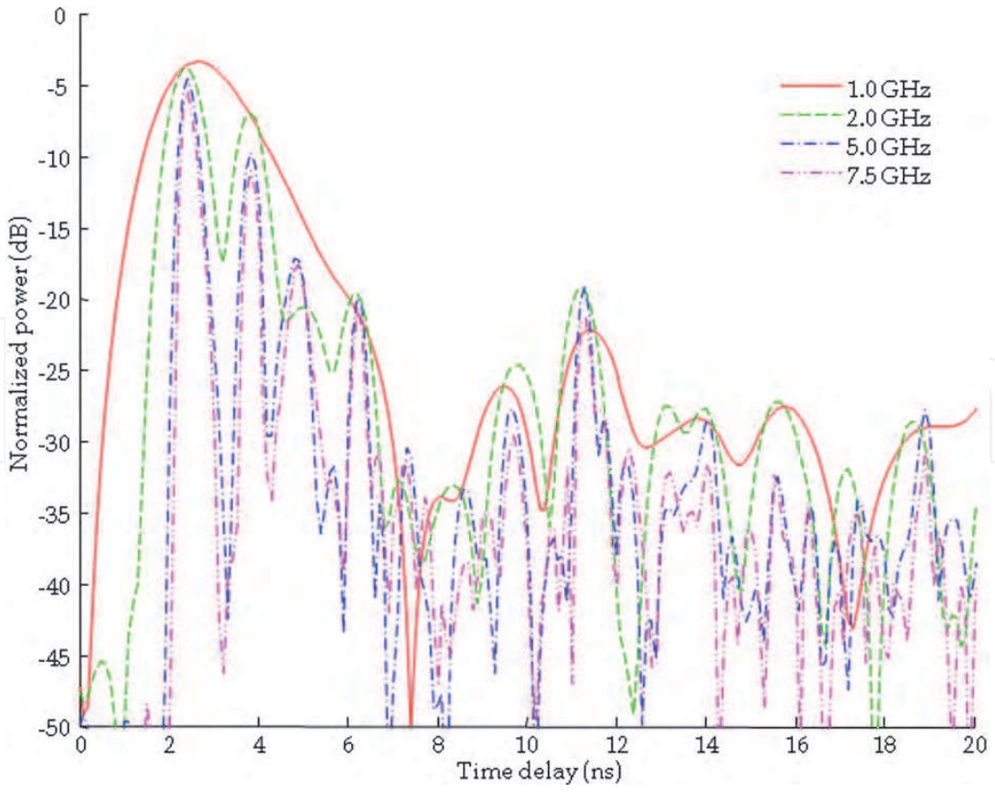

Fig. 7. A detail of normalized power delay profiles at d = 0.78 m for different bandwidths.

3. Path loss

The total path loss is defined as attenuation in the energy of pulse while propagating from the transmitting antenna to the receiving antenna. This can be expressed as a ratio of total energy of the transmitted pulse vs. total energy of the received power delay profile:

$$PL = \frac{\int w^2(t)dt}{\int P_h(t)dt}. \tag{9}$$

The path loss model (Ghassemzadeh at al., 2003) defines the path loss exponent n which characterizes the log-distance dependence and equals 2 for the free space propagation:

$$PL(d) = PL(d_0) + 10 \cdot n \cdot \log(d/d_0) + S, \quad d > d_0, \tag{10}$$

where d is the separation between the transmitter and the receiver, $PL(d_0)$ is the path loss at the reference distance d_0, and S denotes the shadowing term (Section 4).
The total energy received at the Rx antenna is estimated by summing the energy in the entire corrected power delay profile. By subtracting the measured total path loss at a reference distance from this value, we estimate the relative path loss:

$$\overline{PL}[\text{dB}] = PL(d) - PL(d_0)[\text{dB}], \tag{11}$$

where $PL(d)$ presents the path loss estimated from the power delay profile measured at distance d, and $PL(d_0)$ is the measured total path loss at a reference distance, which is selected as d_0 = 0.1 m (see Table 1).
The relative path loss values estimated from the measured power delay profiles are presented on Fig. 8 at different system bandwidths as a function of antenna separation in a logarithmic scale. In this manner the linear regression lines can be fitted into the measurement data using the least square method. The calculated free space path loss line (7) is added for comparison. Note that the correlation coefficient increases while the path loss exponent slightly decreases with increasing bandwidth.
The path loss exponent values estimated in this measurement campaign are comparable to the values found in literature up to date.
A indoor LOS measurement campaign which took place inside an anechoic chamber on a 1.2 m x 0.8 m rectangular aluminum conductive plate simulating a heavy-duty office desk (Suzuki & Kobayashi, 2005) found a path loss exponent value of n = 1.6 using a vertically polarized transmission. This value is lower than the free space path loss exponent (n =2) and the authors attribute this discrepancy to the effects of the diffracted waves from the finite plate edges. The frequency of the UWB signal spanned from 3.1 GHz to 10.6 GHz.
Short range indoor LOS measurements have also been performed in a 6 GHz to 8 GHz frequency band, with a transmitter-receiver distance ranging from 1 m to 5 m (Bose, 2006). A path loss analysis yields a path loss exponent of n = 1.85.
A 3.6 GHz – 6 GHz measurements in 1 m – 11 m range (Cassioli & Durantini, 2004) report a path loss exponent of n = 1.916 for indoor LOS scenarios.
An UWB indoor LOS channel measurement campaign was evaluated in (Cassioli et al, 2001), finding a path loss exponent of n = 2.4.
An extensive research based on analysis of over 300000 power delay profiles measured in 4.375 GHz – 5.625 GHz in various indoor LOS scenarios presented in (Ghassemzadeh et al., 2002) finds the average path loss exponent to have a value of n = 1.7.

Although the frequency dependence analysis of the channel parameters investigated in (Cassioli et al., 2004) resulted in a wide range of path loss exponent values between 0.6 and 2.2 for indoor LOS scenarios, there is no marked dependence on the system bandwidth.

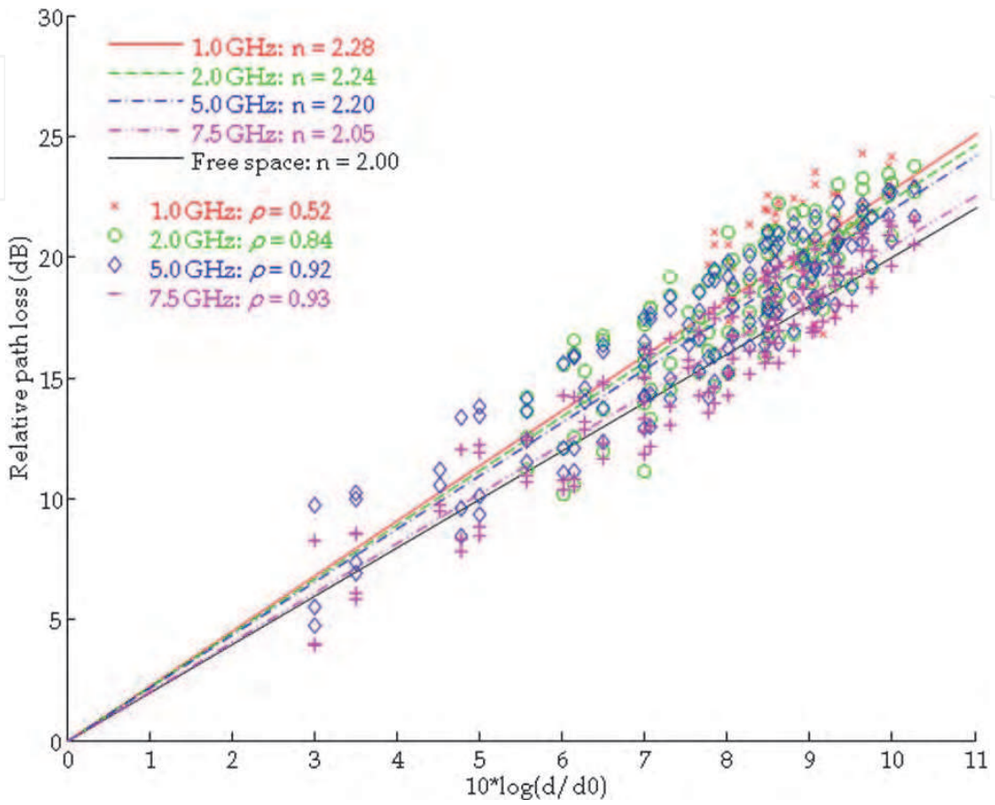

Fig. 8. Scatter plots of the estimated relative path loss vs. logarithm of the normalized distance for different bandwidths. The regression lines represent the path loss power laws.

4. Shadowing

The shadowing term S denotes a zero-mean Gaussian random variable with standard deviation σ, which is estimated from the experimental data:

$$S \sim N(0,\sigma). \tag{12}$$

The shadowing term captures the path loss deviations from its median value.
Fig. 9 presents a comparison of empirical cumulative distribution functions (CDF) of the estimated shadowing term S and theoretical lognormal CDFs with respective standard deviations for different bandwidths, shown in Table 3. For comparison, a far-right column showing the calculated parameter values in free space at central frequency of 6.85 GHz (7) is added.
In a 3.6 GHz – 6 GHz indoor LOS measurements (Cassioli & Durantini, 2004) shadowing is modeled as lognormal, with standard deviation of 1.42 dB for indoor LOS scenarios.

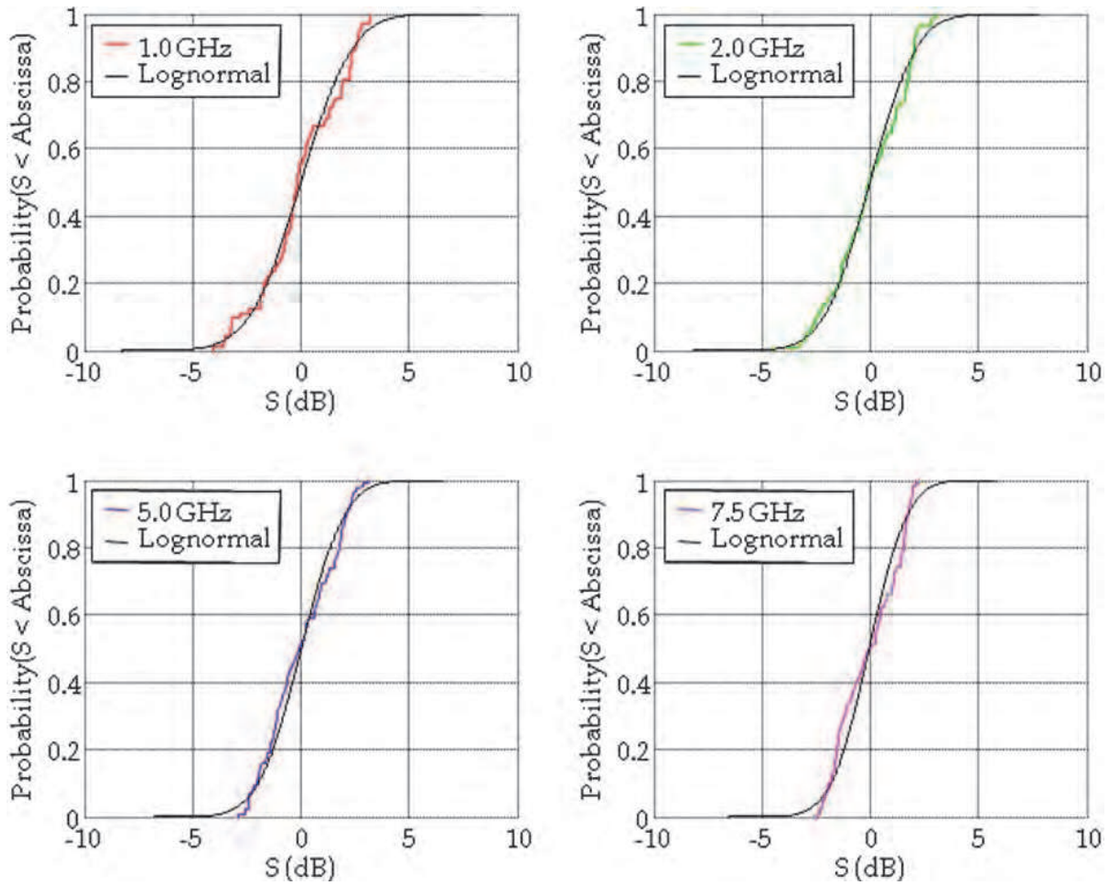

Fig. 9. Empirical CDF of the shadowing term S obtained from the experimental path loss values for different bandwidths. The black line on each CDF represents the theoretical lognormal CDF with the respective calculated standard deviation.

System BW	1 GHz	2 GHz	5 GHz	7.5 GHz	Free space (7)
PL_0	30.12 dB	30.24 dB	29.23 dB	28.63 dB	29.16 dB
n	2.28	2.24	2.2	2.05	2
σ	1.87 dB	1.67 dB	1.57 dB	1.39 dB	0 dB

Table 3. Measured path loss at a reference distance d = 0.1 m, path loss exponents n and standard deviations of the shadowing term S for different bandwidths. Note that the standard deviation of the shadowing term S decreases as the bandwidth increases.

An UWB indoor LOS channel measurement campaign was evaluated in (Cassioli et al, 2001), finding standard deviation of shadowing term of 5.9 dB.
An extensive research based on analysis of over 300000 power delay profiles measured in 4.375 GHz – 5.625 GHz for indoor LOS scenarios presented in (Ghassemzadeh et al., 2002) reports on the standard deviation of the shadowing term of 1.6 dB.

5. Mean excess delay

Mean excess delay is commonly used to describe the time dispersion characteristics of a transmission channel. It is defined as the first moment of the power delay profile:

$$\bar{\tau} = \frac{\int_0^\infty t P_h(t)\,dt}{\int_0^\infty P_h(t)\,dt}. \tag{13}$$

The scatter plot of the mean excess delay values, estimated according to (13) from the measured power delay profiles, is presented on Fig. 10 in dependence on the antenna separation for different bandwidths.
Fig. 11 presents a scatter plot of the estimated mean excess delay in function of the estimated total path loss for different bandwidths. We find a significant correlation between these two parameters, which is slightly increasing with the bandwidth.

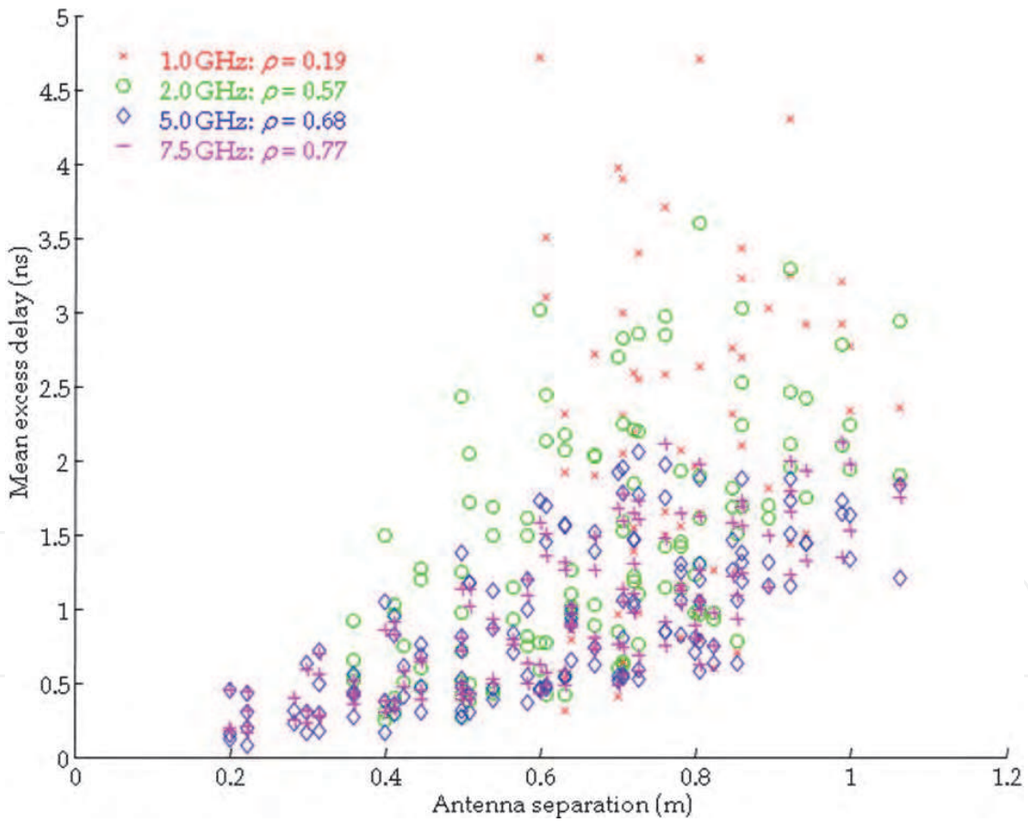

Fig. 10. Scatter plot of estimated mean excess delay vs. antenna separation for different bandwidths. Note that the correlation between these two estimated parameters increases with bandwidth.

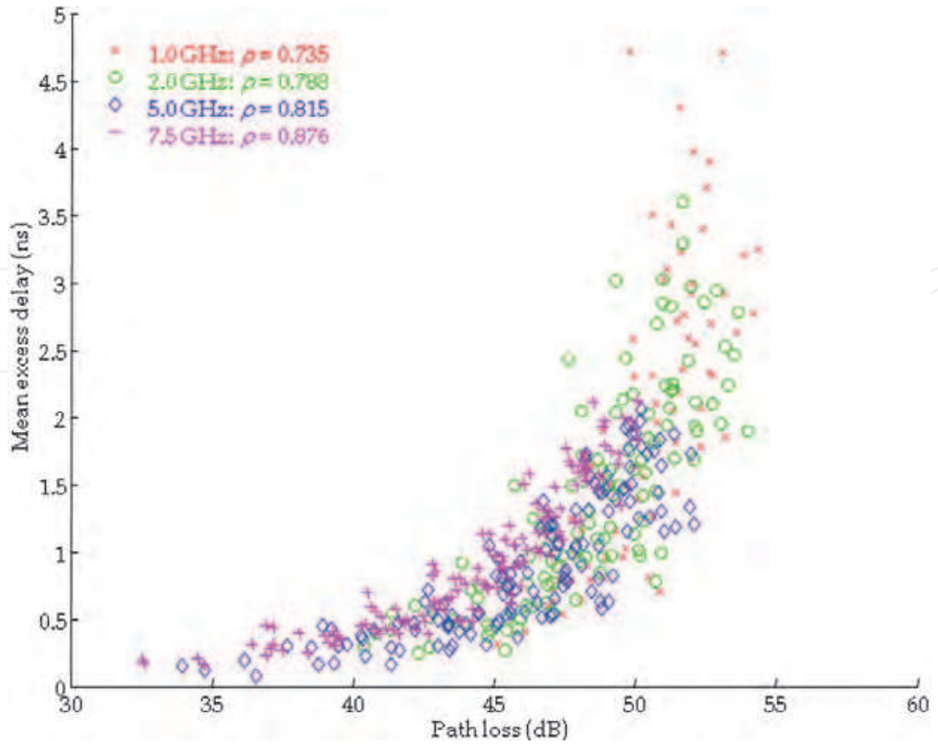

Fig. 11. Scatter plot of estimated mean excess delay vs. estimated total path loss for different bandwidths. Note the slight increase in correlation for larger bandwidths.

6. RMS delay spread

RMS delay spread is another parameter that characterizes the time dispersion of the channel. It is defined as a square root of the second central moment of the power delay profile:

$$\tau_{RMS} = \sqrt{\frac{\int_0^{\infty} \left(t-\bar{\tau}\right)^2 P_h(t)\,dt}{\int_0^{\infty} P_h(t)\,dt}}. \tag{14}$$

As omitting the subtraction of the RMS delay spread of the calibrated pulse would yield overestimated results (Varela & Sánchez, 2001), in order to estimate the RMS delay spread it is necessary to subtract the RMS delay spread of the calibrated pulse from the RMS delay spread of each measured PDPs (Saleh & Valenzuela, 1987):

$$\tau_{RMSest} = \tau_{RMSmeas} - \tau_{RMSpulse}, \tag{15}$$

where $\tau_{RMSmeas}$ is the RMS delay spread estimaed from the measured power delay profile (14) and $t_{RMSpulse}$ is the estimated RMS delay spread value of the calibrated pulse at a given bandwidth (Table 2). The results show a certain dependence on the antenna separation, where the correlation coefficient rises as the bandwidth increases (Fig. 12).

Fig. 13 presents a comparison of empirical cumulative distribution functions (CDF) of the estimated RMS delay spread values and theoretical normal CDFs with respective standard deviations for different bandwidths, shown in Table 4. Note that the mean value of the estimated RMS delay spread values decreases with increasing bandwidth.

System BW	1 GHz	2 GHz	5 GHz	7.5 GHz
Mean	5.93 ns	4.85 ns	3.85 ns	3.9 ns
Std. dev.	1.37 ns	1.37 ns	1.25 ns	1.36 ns

Table 4. Mean values and standard deviations of estimated RMS delay spread values for different bandwidths.

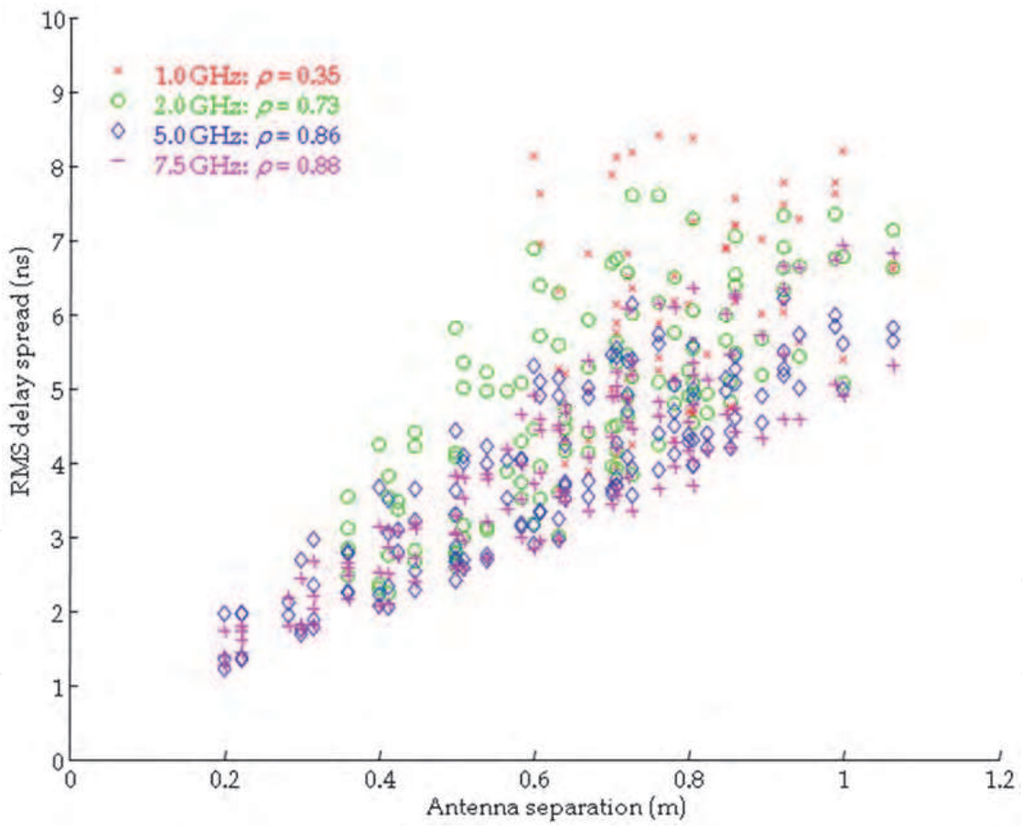

Fig. 12. Scatter plot of estimated RMS delay spread vs. antenna separation for different bandwidths. Note that the correlation coefficient increases with the bandwidth.

An extensive research based on analysis of over 300000 power delay profiles measured in 4.375 GHz – 5.625 GHz presented in (Ghassemzadeh et al., 2002) reports on normally distributed mean excess delay and RMS delay spread with mean value of 4.7 ns and standard deviation of 2.3 ns for indoor LOS scenarios. This increase is explained to be largely due to paths with longer delays having larger path loss values associated with them. Fig. 14 presents a scatter plot of estimated RMS delay spread in dependence of the total path loss. It is evident that these two parameters are strongly correlated.

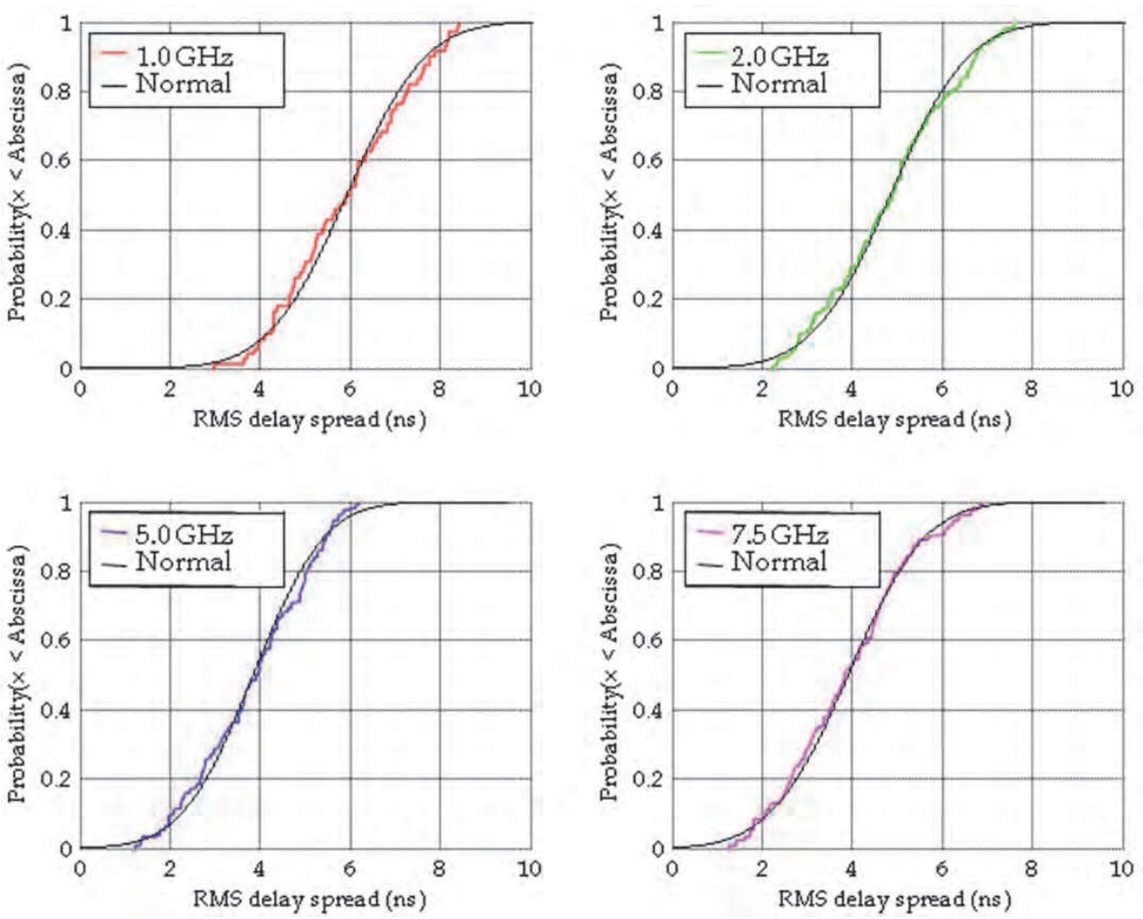

Fig. 13. Empirical CDF of estimated RMS delay spread obtained for different bandwidths. The black line on each CDF represents the theoretical normal CDF with the respective calculated mean and standard deviation.

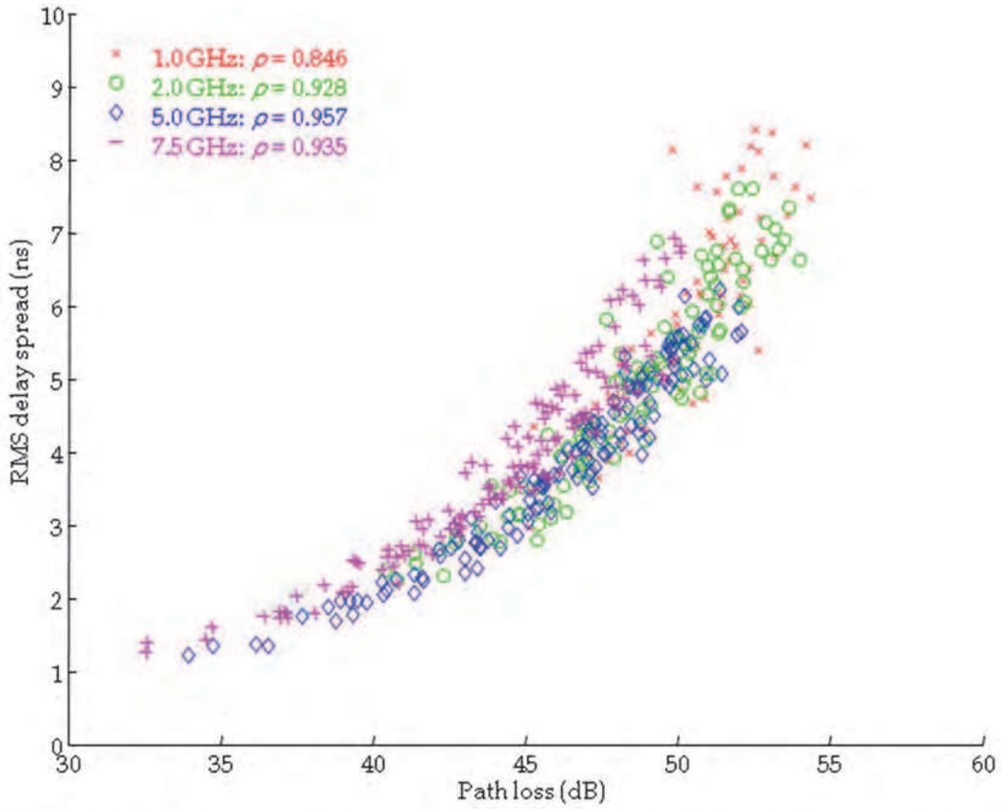

Fig. 14. Scatter plot of estimated RMS delay spread vs. estimated total path loss for different bandwidths.

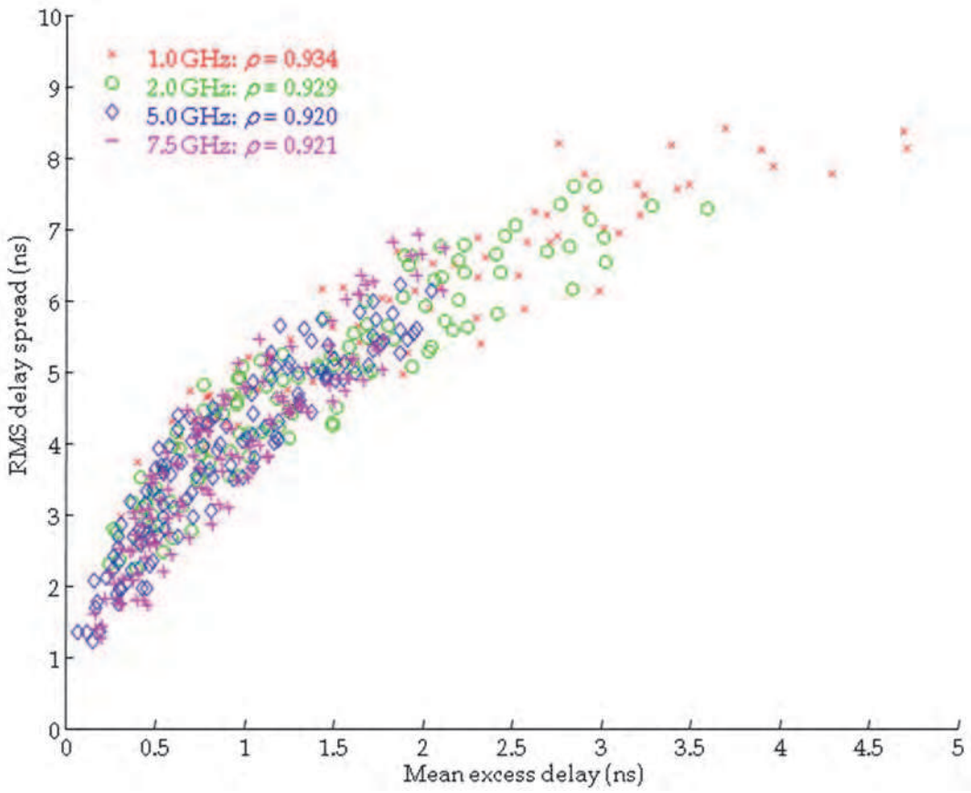

Fig. 15. Scatter plot of estimated RMS delay spread vs. estimated mean excess delay for different bandwidths.

A scatter plot of estimated RMS delay spread in function of the estimated mean excess delay is presented on Fig. 15. A strong correlation is observed for all bandwidths.

7. Discussion

The research presented in this chapter showed a certain dependence of the estimation of channel parameters on the system bandwidth.

First, the estimated path loss exponent slightly decreases with increasing the system bandwidth. An explanation can be found in the frequency selective propagation mechanisms, since different frequency components experience different impact of diffraction, reflection and transmission, where the coefficients that define these processes are dependent on the frequency of the transmitted signal. The estimated path loss exponent is slightly higher than the free space path loss exponent (between 2.05 and 2.28 for different bandwidths). Considering that the path loss exponent estimates for UWB indoor scenarios found in the literature are regularly below 2, the additional loss in the presented measurement campaign might be explained by the influence of the used desk, made of wood, chipboard and MDF.

Second, the estimated standard deviation of the shadowing term evidently decreases with increasing the system bandwidth, which in turn causes the increase in correlation between the estimated total path loss and antenna separation. This can also be explained as a direct consequence of the frequency selective propagation mechanisms. At larger bandwidths,

more frequency components will be immune to reflections and diffraction, so that the received signal will be more consistent.
Third, the estimated RMS delay spread decreases with increasing the system bandwidth, because the system with wider spectrum is able to resolve more multipath components.
It is shown that estimated correlations between the various channel parameters investigated in this research are greater as the system bandwidth increases. This is obviously another consequence of better temporal resolution in due to shorter pulses at wider bandwidths.

8. Conclusion

The main scope of this chapter was to explore the validity of well established empirical methods used for UWB channel modeling and to propose the estimated values of the model parameters for a specific propagation environment.
An indoor UWB measurement campaign presented in this chapter was performed on an empty surface of a desk placed in a typical office room. The channel impulse responses were measured on the surface of the desk at different system bandwidths using a VNA method. The channel parameter values were estimated from the measurement results for each different bandwidth. The estimated values are comparable with the ones found in literature.
Analyzing the estimated values we have found that the estimations of the channel parameters show a certain dependence on the system bandwidth. The estimated path loss exponent values, standard deviations of the shadowing term, RMS delay spread mean values and mean excess delay values are all decreasing with increasing bandwidth for this indoor LOS scenario.
The analysis of correlation between the estimated values showed that the correlation coefficients tend to be higher at wider bandwidths.

9. Acknowledgment

The authors wish to thank Prof. A. Šarolić and Mr. Z. Živković for use of their GTEM cell and assistance in measuring the antennas' radiation patterns.

10. References

Bose, R. (2006). Ultra Wideband Channel Modeling for Personal Area Network, *Proceedings of First European Conference on Antennas and Propagation (EuCAP 2006),* pp. 1-4, ISBN 978-92-9092-937-6, Nice, France, 6-10 November 2006

Cassioli, D. & Durantini, A. (2004). A time-domain Propagation Model of the UWB Indoor Channel in the FCC-compliant Band 3.6 – 6 GHz based on PN-sequence Channel Measurements, *Proceedings of IEEE 59th Semiannual Vehicular Technology Conference (VTC '04)*, Vol. 1, pp. 213-217, ISBN 0-7803-8255-2, Milan, Italy, 17-19 May 2004

Cassioli, D., Durantini, A. & Ciccognani, W. (2004). The Role of Path Loss on the Selection of the Operating Bands of UWB Systems, *Proceedings of IEEE 15th International Symposium on Personal, Indoor and Mobile Radio Communications (PIMRC 2004)*, Vol. 4, pp. 2787-2791, ISBN 0-7803-8523-3, Barcelona, Spain, 5-8 September 2004

Cassioli, D., Win, M.Z. & Molisch, A.F. (2001). A Statistical Model for the UWB Indoor Channel, *Proceedings of IEEE 53rd Vehicular Technology Conference (VTC '01)*, Vol. 2, pp. 1159-1163, ISBN 0-7803-6728-6, Rhodes, Greece, 6-9 May 2001

Chang, W.-J. & Tarng, J.-H. (2007). Effects of Bandwidth on Observable Multipath Clustering in Outdoor/Indoor Environments for Broadband and Ultrawideband Wireless Systems, *IEEE Transactions on Vehicular Technology*, Vol. 56, No. 4, (July 2007), pp. 1913-1923, ISSN 0018-9545

Choi, J., Kang, N.-G., Sung, Y.-S., Kang, J.-S. & Kim, S.-C. (2009). Frequency-Dependent UWB Channel Characteristics in Office Environments, *IEEE Transactions on Vehicular Technology*, Vol. 58, No. 7, (September 2009), pp. 3102-3111, ISSN 0018-9545

Ghassemzadeh, S.S., Greenstein, L.J., Kavcic, A., Sveinsson, T. & Tarokh, V. (2003). An Empirical Indoor Path Loss Model For Ultra-Wideband Channels, *Journal of communication and networks,* Vol. 5, No. 4, (December 2003), pp. 303-308, ISSN 1229-2370

Ghassemzadeh, S.S., Greenstein, L.J., Sveinsson, T., Kavcic, A. & Tarokh, V. (2005). UWB Delay Profile Models for Residential and Commercial Indoor Environment, *IEEE Transactions on Vehicular Technology*, Vol. 54, No. 4, (July 2005), pp. 1235-1244, ISSN 0018-9545

Ghassemzadeh, S.S., Jana, R., Tarokh, V., Rice, C.W. & Turin, W. (2002). A Statistical Path Loss Model for In-home UWB Channels, *Proceedings of IEEE Conference in Ultra Wideband Systems and Technologies (UWBST '02)*, pp. 59-64, ISBN 0-7803-7496-7, Baltimore, Maryland, USA, 21-23 May 2002

Hewlett-Packard Company (1989). Time and Frequency Domain Transforms, In: *HP 8719A, HP 8720B Microwave Network Analyzer Operating Manual*, Hewlett-Packard Company, Santa Rosa, California, USA

Hovinen, V., Hämäläinen, M., & Pätsi, T. (2002). Ultra Wideband Indoor Radio Channel Models: Preliminary Results, *Proceedings of IEEE Conference in Ultra Wideband Systems and Technologies (UWBST '02)*, pp. 75-79, ISBN 0-7803-7496-7, Baltimore, Maryland, USA, 21-23 May 2002

Molisch, A.F. (2005). Ultrawideband Propagation Channels-Theory, Measurement and Modeling, *IEEE Transactions on Vehicular Technology*, Vol. 54, No. 5, (September 2005), pp. 1528-1545, ISSN 0018-9545

Molisch, A.F. (May 31, 2006). UWB Propagation Channels, In: *UWB Communication Systems: A Comprehensive Overview,* Di Benedetto, M.-G., Kaiser, T., Molisch, A.F., Opperman, I., Politano, C. & Porcino, D., pp. 21-118, Hindawi Publishing Corporation, ISBN 977-5945-10-0, New York, USA

Saleh, A.A.M., & Valenzuela, R.A. (1987). A Statistical Model for Indoor Multipath Propagation. *IEEE Journal on Selected Areas in Communications*, Vol. 5, No.2, (February 1987), pp. 128-137, ISSN 0733-8716

Suzuki, Y. & Kobayashi, T. (2005). Ultra Wideband Signal Propagation in Desktop Environments, *IEICE Transactions on Fundamentals of Electronics, Communications and Computer Sciences*, Vol. E88-A, No. 9, (September 2005), pp. 2272-2278, ISSN: 0916-8508

Taniguchi, T., Maeda, A. & Kobayashi, T. (2006). Development of an Omnidirectional and Low-VSWR Ultra Wideband Antenna, *International Journal on Wireless & Optical Communications*, Vol. 3, No. 2, (August 2006), pp. 145-157, ISSN 0219-7995

Varela, M.S. & Sánchez, M.G. (2001). RMS Delay and Coherence Bandwidth Measurements in Indoor Radio Channels in the UHF Band, *IEEE Transactions on Vehicular Technology*, Vol. 50, No. 2, (March 2001), pp. 515-525, ISSN 0018-9545

Živković, Z. & Šarolić, A. (2010). Measurements of Antenna Parameters in GTEM cell. *Journal of Communications Software and Systems*, Vol. 6, No. 4, (December 2010), pp. 125-132, ISSN 1845-6421

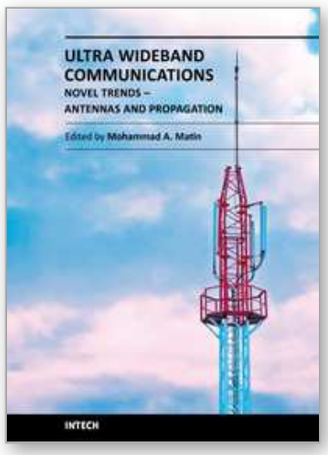

Ultra Wideband Communications: Novel Trends - Antennas and Propagation

Edited by Dr. Mohammad Matin

ISBN 978-953-307-452-8
Hard cover, 384 pages
Publisher InTech
Published online 09, August, 2011
Published in print edition August, 2011

This book explores both the state-of-the-art and the latest achievements in UWB antennas and propagation. It has taken a theoretical and experimental approach to some extent, which is more useful to the reader. The book highlights the unique design issues which put the reader in good pace to be able to understand more advanced research.

How to reference

In order to correctly reference this scholarly work, feel free to copy and paste the following:

Duje Ćoko, Zoran Blažević and Ivan Marinovic (2011). Effects of Bandwidth on Estimation of UWB Channel Parameters, Ultra Wideband Communications: Novel Trends - Antennas and Propagation, Dr. Mohammad Matin (Ed.), ISBN: 978-953-307-452-8, InTech, Available from: http://www.intechopen.com/books/ultra-wideband-communications-novel-trends-antennas-and-propagation/effects-of-bandwidth-on-estimation-of-uwb-channel-parameters

INTECH
open science | open minds

InTech Europe
University Campus STeP Ri
Slavka Krautzeka 83/A
51000 Rijeka, Croatia
Phone: +385 (51) 770 447
Fax: +385 (51) 686 166
www.intechopen.com

InTech China
Unit 405, Office Block, Hotel Equatorial Shanghai
No.65, Yan An Road (West), Shanghai, 200040, China
中国上海市延安西路65号上海国际贵都大饭店办公楼405单元
Phone: +86-21-62489820
Fax: +86-21-62489821

IntechOpen